ACS OMEGA

Open Access

http://pubs.acs.org/journal/acsodf

Article

Insights into Molecular Dynamics and Oil Extraction Behavior of the Polymeric Surfactant in a Multilayered Heterogeneous Reservoir

Hao Zheng, Huiqing Liu,* and Kaijun Tong

Cite This: *ACS Omega* 2024, 9, 11243−11254

Read Online

ACCESS | Metrics & More | Article Recommendations

ABSTRACT: Interlayer heterogeneity, an inevitable and complex challenge during water flooding, seriously constrains the spread of the sweep region and oil recovery enhancement in multilayered heterogeneous reservoirs. To overcome this challenge, a novel polymeric surfactant, having an excellent performance in the reduction of interfacial tension (IFT) and the increase of viscosity of displacing fluid, is applied for enlarging the sweep resonance and increasing the oil washing efficiency. Through the molecular dynamics (MD) simulation, the molecular distributing mechanisms of the polymeric surfactant at the oil−water interface are analyzed to provide the theoretical basis for explaining the microscopic mechanism of oil extraction. To directly reflect the microscopic behavior of oil extraction, multiple transparent sand-packed models are designed to investigate the flowing behavior of different fluids and the extracted mechanisms of the remaining oil in both pore and macroscales. The multilayered heterogeneous reservoirs consisting of high-, moderate-, and low-permeability layers are fabricated to represent a heterogeneous characteristic. The recognition from the visual experiment and MD simulation can study the performance control, the extracting performance of the remaining oil, and the expression of the displacing front from different perspectives. The results from MD simulation demonstrate that the polymeric surfactant can promote the disintegration of the remaining oil and enhance its mobility. The experimental results indicate that the sweep efficiency is restricted by viscous fingering and tongue advance. Through the analysis of mathematical models, the rising mobility ratio and the location of the displacing front have a strong positive relationship with viscous fingering and tongue advance, which can reasonably explain the plugging performance of the polymeric surfactant, greatly improving the sweeping effect of the whole reservoir. Moreover, the Marangoni effect generated by the IFT gradient can induce the transformation of interfacial energy to displacement kinetic energy by the emulsification of the oil−water interface so that the remaining oil in the blind-end pore can be effectively extracted. However, by comparing data from image quantification techniques and production dynamic performance, the sweep efficiency (484%) was significantly greater than that of oil recovery (300%), demonstrating that the expanded sweep effect still plays a dominant role in the extraction of remaining oil after polymeric surfactant flooding. This study provides a novel plugging and effective washing agent that is expected to be an excellent and comprehensive method for solving the problem of low oil recovery in multilayered heterogeneous reservoirs.

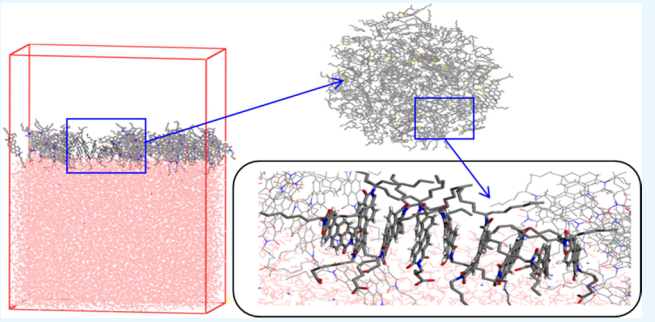

INTRODUCTION

Heterogeneous characteristics of reservoirs, as one of the universal and toughest problems, severely constrains the enhancement of oil recovery (EOR).[1,2] Moreover, the heterogeneity can be divided into two types based on whether the fluid flowing in different regions is induced by interlayers: interlayer heterogeneity and intralayered heterogeneity. Intralayered heterogeneity only denotes that the regions with different permeabilities and porosities exist in the same layer, and interlayer heterogeneity is mainly caused by the barrier of interlayers so that no fluid exchanges in different layers.[3,4] The heterogeneity can be exacerbated by the long-term scouring of injected fluid with low viscosity, causing the remaining oil to be left in the unswept region.[5] Therefore, the key to enhance oil recovery of multilayered heterogeneous reservoirs is optimizing the sweep effect among different layers and enhancing the remaining oil from the poor connectivity pores in the sweep region.[6]

To solve the problem of poor performance on sweep effect caused by heterogeneity, many experts put froward a variety of oil extraction schemes. He et al. have proposed a mature technology on separating layer water injection to keep long-term

Received: August 27, 2023
Revised: December 20, 2023
Accepted: December 22, 2023
Published: February 27, 2024

Table 1. Mineral Composition of Formation Water

type of ions	Na^+	Mg^{2+}	Ca^{2+}	CO_3^{2-}	HCO_3^-	Cl^-	SO_4^{2-}	Total
concentration of ions (mg/L)	9121	152.2	320.2	2726.2	11606.4	4452.6	250.8	28629.4

high and stable production of oilfields.[7] Furthermore, the optimization control of injection production by down hole separators from the inlet of reservoirs greatly improves the development of adsorption profile among different layers.[8,9] Another effective technology is the method of tertiary recovery to adjust the flow profile.[10,11] Multiple chemical fluids, such as surfactant−polymer (SP) flooding, alkali-surfactant−polymer (ASP) flooding, hybrid steam-chemical flooding, colloidal dispersion gel flooding, nanomaterial flooding, and so on, sealing the flow channels and altering the flow capacity of oil are regarded as important criteria for chemical fluid selection. SP flooding and ASP flooding can reduce the oil−water interfacial tension (IFT), thereby weakening the seepage resistance of the oil phase.[12−14] Steam-assisted chemical flooding can reduce the viscosity of heavy oil and promote the wettability on the rock surface to hydrophilic direction[15,16] studied that colloidal dispersion gel flooding can directly block the flow channels generated by primary water flooding, so as to force subsequent fluid into the unswept region. Nanomaterials flooding can achieve the goal of decrement in the viscosity of heavy oil, reduction of oil−water IFT, and alteration of wettability.[17] Based on the profile control by chemical fluids, the heterogeneity can be weakened, and the swept region can be obviously enlarge. However, the detailed performance of sweep effect in different layers, such as oil saturation field, distribution, and flow mechanisms of different fluids, needs further description.

To solve the problem of poor performance on oil washing caused by the pore structure in the flow channels, some researchers recognized that immobile oil can be extracted by multiple mechanisms of injected fluids. SP and ASP flooding improve the mixing flow capacity of oil−water.[18] In addition, the alteration of IFT enhances the transfer of interfacial materials (convection, diffusion, and adsorption−desorption) and results in the unstable extraction phenomenon, termed the "kicking drop" by some experts.[19,20] A series of self-propelled behaviors of active materials can be triggered by the alteration of IFT, which is usually regarded as the Marangoni effect to drive fluid migration.[21] Marangoni effect is a wide phenomenon of fluid mass transfer and promotes the extraction of the remaining oil.[22,23] In addition to the surfactant, the polymer performs a pulling effect to attract oil away from the low-connectivity pore.[24] However, it is also a tricky problem to observe the microscopic processes to extract the remaining oil in porous media. However, observing the microscopic processes on pulling effect of polymer in porous media is also a tricky problem.[25,26]

The mobility of oil at an interface is governed by its viscosity and the interfacial properties between the oil and water. From the molecular point of view, the distribution and transportation of oil and external fluids play a pivotal role in determining the interfacial behavior.[27,28] Interactions between oil and additives can facilitate the propagation of a microscopic displacement front. However, understanding the interactions between the oil and polymer−surfactant fluid molecules and elucidating the mechanisms behind complex multicomponent interactions in reservoir conditions pose significant challenges.[29] Moreover, the properties of the formation fluid and the past operational strategies further complicate the selection of an appropriate combination of polymer−surfactant fluids.

To directly and accurately analyze the flow behavior and mechanism, selecting appropriate tools is crucial. Some experts have put forward different models to load the production dynamics data and describe the distributed tendency of different fluids. Wu et al. employed multi sand-packed pipes, as a one-dimensional model, to investigate the blockage and fluid diversion behaviors of the polymer.[30] Other experts studied the migration of different chemical fluids through two-dimensional visual models and three-dimensional (3D) detectable models and obtained positive performance to reflect the flow mechanisms in porous media.[31,32] Previous experiments in various dimensions have been able to demonstrate the fluid mass transfer in porous media at both macroscopic and microscopic scales.[33] Nevertheless, the quantitative analysis of fluid distribution and mathematical models of fluid migration still need to be supplemented.

In this work, molecular dynamics (MD) simulation is employed to explain the dynamic behavior of polymeric surfactants at the oil−water interface. Moreover, the IFT, contact angle, and cryo-scanning electron microscopy are examined to analyze the microscopic properties of the polymeric surfactant.[34] Displacement experiment, containing multiple sand-packed models to simulate multilayered heterogeneous reservoirs, is applied to verify the performance of oil extracted by the polymeric surfactant. Based on the experiments, mathematical models are employed to investigate the displacing front. In detail, tongued advance and viscous fingering in heterogeneous reservoirs are deduced, as well as the influence factors. Then, comparative research in brine, polymeric surfactant, and typical anionic surfactant was carried out to extract oil from different layers. Finally, the types of remaining oil and its extraction mechanism by the polymeric surfactant are studied from a microscopic perspective. After discussing the effects of oil washing and sweep expanding on the macro- and microviews, the polymeric surfactant proposed in this work is expected to be an appropriate agent to solve the common problem of low sweep efficiency by water channeling in multilayered heterogeneous reservoirs.

EXPERIMENTAL MATERIALS AND METHODOLOGY

Experimental Materials. *Reservoir Fluids.* The original fluids used in the experiment are crude oil and brine. The salinity of brine was measured at 2.86×10^4 mg/L as shown in Table 1. The viscosity and density (degassed) of heavy oil were 63 mPa s and 0.956 g/cm^3 at 55 °C.

Chemical Agent. The polymeric surfactant by the Research Institute of Petroleum Exploration and Development can enhance the viscosity of brine and reduce the IFT to 3×10^{-3} mN/m. The viscosity of the solution of polymeric surfactant was 83 mPa s at 55 °C and 500 ppm.

On the comparative research on polymeric surfactants, an anionic surfactant (sodium dodecyl benzenesulfonate, SDBS) is injected after polymeric surfactant flooding. In some works by other researchers, the anionic surfactant has a favorable performance on flow stability, wettability alteration, and IFT reduction in the sand-packed model. Therefore, it is reasonable

https://doi.org/10.1021/acsomega.3c06390
ACS Omega 2024, 9, 11243−11254

to use SDBS as the contrast chemical agent of polymeric surfactants.[35] The concentration of 200 mg/L was selected for the displacement experiment and tests.

Model. In this work, the visual sand-packed model consists of two glass plates with the length of 25 cm.[36] The visual sand-packed model comprises machine parts represented by glass beads, simulating the rock skeleton, and thermal-resistant colloids, simulating formation cements. In particular, one of the glass plates is equipped with four penetrating holes to simulate the wellbores as shown in Figure 1.

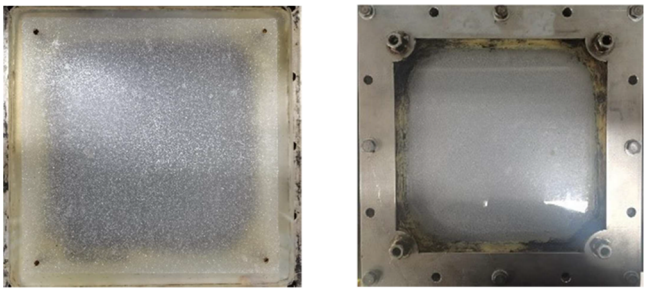

(a) The interior top view (b) The external top view

Figure 1. Images of the structure of the visual sand-packed model.

The three models are filled with different sizes of glass beads, including 20 mesh (830 μm), 30 mesh (550 μm), and 40 mesh (380 μm), simulating the multilayered heterogeneous reservoir. The glass beads are fabricated by Dongguan Jinying Abrasive Technology Co., Ltd., which have the characteristics of great pressure resistance and good chemical stability. The glass beads are evenly packed in the sand-packed model, measuring the porosity by the volume method. The permeability of the sand-packed model is estimated by the rhomboidal structure diameter using the following equation:[37]

$$K = \frac{{d_m}^2}{180} \cdot \frac{\phi^3}{(1-\phi^2)} \quad (1)$$

where d_m is the size of glass beads and ϕ is the porosity of the sand-packed model. After multiple sand-packed models are completed, the porosity (pore diameter) and maximum diameter of the pore (pore diameter) of different layers are shown in Table 2.

Table 2. Parameters of the Three-Piece Sand-Packed Models

HPL		MPL		LPL		
Poro. (%)	Pd. (μm)	Poro. (%)	Pd. (μm)	Poro. (%)	Pd. (μm)	maximum diameter of pore
35.4	244.69	29.7	177.04	26.2	96.41	1.89:1.21:1.00

Experimental Apparatus. The schematic diagram of the experimental apparatus is shown in Figure 2. Three pieces of visual sand-packed models are placed in the incubator to maintain the temperature of the reservoir. The information acquisition system contains a digital camera microscope and a full HD camera. The digital camera microscope produced by Sweden Optilia company can magnify the visible region (the largest magnification is 200 times) to capture microscopic images.[38] Production data including pressure and producing volume of the liquid can be continuously collected.

Experimental Process. The detailed displacement procedures are presented as follows:

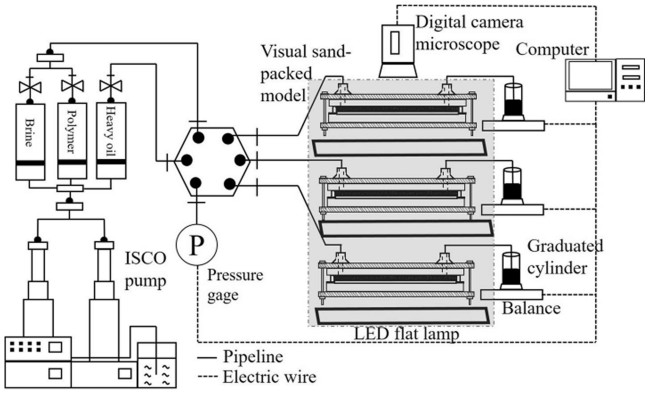

Figure 2. Schematic diagram of the experimental apparatus.

(1) Establishment of the experimental system: The experimental devices were connected, and their air tightness was checked. The incubator was set to 55 °C to simulate the temperature of the reservoir.

(2) Saturation of brine: Brine was injected into different layers by the ISCO pump at a flow velocity of 0.5 mL/min until the brine could flow steadily from the outlet. Meanwhile, the porosity of different layers can be measured by the volume method by the following equation:

$$\phi = \frac{V_B}{L \times H \times W} \times 100\% \quad (2)$$

where ϕ is the porosity of model, V_B is the volume of the injected fluid, L is the length of the layer, H is the thickness of the layer, and W is the width of the layer. After all visual sand-packed models are saturated with brine, every valve connected with the model can be opened to obtain the producing brine ratio in the different models.

(3) Saturation of oil: Oil was injected into the three sand-packed models separately by the ISCO pump at a flow velocity of 0.25 mL/min until the oil could flow steadily from the outlet of models. And then, all valves in the six-way valve were closed.

(4) Aging of simulated reservoir: All sand-packed models are fully saturated oil, and then these are put in the incubator at 55 °C for more than 168 h. The heterogeneous reservoirs can be constructed and divided into high-permeability layer (HPL), moderate- permeability layer (MPL), and low-permeability layer (LPL) as shown in Figure 3.

(5) Primary extraction period (hot brine): Hot brine (55 °C) was injected into the simulated reservoir at a flow velocity of 0.25 mL/min until the total water fraction reached 90%.

(6) Subsequent extraction period (polymeric surfactant solution): Polymeric surfactant solution was injected at a flow

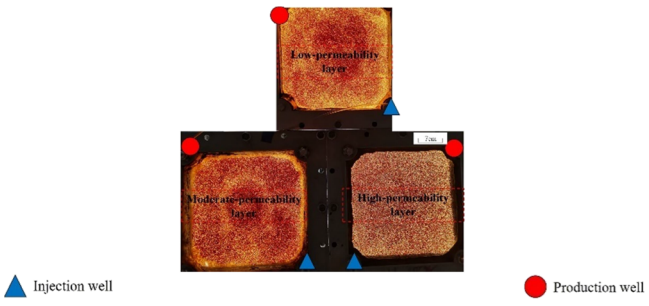

Figure 3. Initial state of the heterogeneous simulated reservoir.

https://doi.org/10.1021/acsomega.3c06390
ACS Omega 2024, 9, 11243−11254

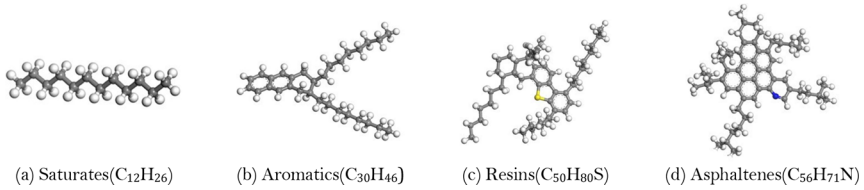

Figure 4. Molecular structures of the different components.

velocity of 0.25 mL/min until the injected volume was 0.05 pore volume (PV).

(7) Successive extraction period (hot brine): Hot brine was injected at a flow velocity of 0.25 mL/min until the volume of total water fraction reached 90% again.

(8) Deep processing on images: After three extraction periods, macroscopic distribution images of different fluids can be obtained. At different periods, the characteristics of microscopic remaining oil in the swept region greatly vary. Through deep processing on oil−brine distributed images, the variable characteristics of the remaining oil in some water channels and unswept regions can directly reflect the effect of the polymeric surfactant.

(9) Ultimate extraction period (SDBS solution): SDBS was injected at a flow velocity of 0.25 mL/min until the injected volume of the water fraction reached 90% again.

MD simulation. *Molecular Model.* In this work, MD simulation was applied to study the microscopic adsorption mechanism of the polymeric surfactant and SDBS at the oil−brine interface by the interaction between chemical groups and components from oil (brine has some Na^+ and Cl^-). To accurately reproduce the actual process, two molecular models containing different chemical agents in oil−water system were constructed.

According to the composition of the oil sample, a comprehensive SARA (saturates, aragonomics, resins, and asphaltenes) model is employed to investigate the effect of reduction in the IFT on the oil−brine interface. Based on the average SARA component model, the asphaltenes are the crucial components on the IFT.[39] Thus, the improved Yen-Mullins asphaltene model is suitable for the adsorption at the oil−brine interface.[40] The structures of different components are shown in Figure 4. Taking into account the actual condition, the shape of the oil model is optimized to be spherical, and the SARA fraction ratio is set as 4:3:1:1.[41]

The construction process of the 3D periodic molecular model is as follows: (1) The geometric optimizations of the oil model are conducted by a smart algorithm employed with 20,000 iterations. (2) MD simulation of the oil model was set as 5 ns to complete the relaxation process so that it can be obtained the reasonable equilibrium configuration. (3) A polymeric surfactant or SDBS layer and pure water layer are added in the $x-y$ horizontal size of a simulated box of 2.22 nm × 7.25 nm. The MD simulation was optimized by 10 ps to mix the chemical agent layer with a pure water layer. Specially, this optimization process was not the formal MD simulation. (4) Based on the oil simulation, the optimized chemical agent layer and the pure water layer were added to construct the oil−water interfacial model, and a 1.5 nm vacuum layer was added on the top of simulation box as shown in Figure 5. (5) The initial oil−water interfacial model was iterated by a maximum descent algorithm to obtain the optimal system structure. Then, this system was minimized by the conjugate gradient algorithm to obtain the system structure with minimum energy.

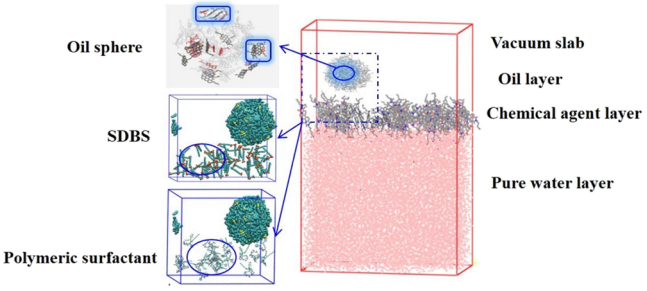

Figure 5. Production data of the total period in the heterogeneous reservoir.

Molecular Potential. Due to the three different fluids in the oil−brine molecular model, different fluids have different potential methods to calculate the alteration of energy and coordinates during the MD simulation. It is important for accurate MD to select the types of force field and interaction parameters for potential energy.[42] The OPLS-AA as an all-atomic force field applied in computer modeling of many organic compounds, such as alkanes, polymers, and biological macro-molecules, is employed to obtain the characteristics of chemical agents and oil model.[43,44] The OPLS-AA force field of the oil−brine interfacial model employs the Lorentz−Berthelot mixing rule to calculate the LJ potential energy, which can be expressed as $\varepsilon_{ij} = \sqrt{\varepsilon_{ii}\varepsilon_{jj}}$ and $\sigma_{ij} = (\sigma_{ii} + \sigma_{jj})/2$, and its cutoff distance is set as 1.2 nm. The mathematical formula of the total potential energy of the OPLS-AA force field can be expressed as

$$U_{total} = U_s + U_u + U_t + U_{nb} \tag{3}$$

$$U_s = \sum_{bonds} k_s(l - l_0)^2 \tag{4}$$

$$U_b = \sum_{angles} k_b(\theta - \theta_0)^2 \tag{5}$$

$$U_t = \frac{1}{2}\sum_{torsion} \{V_{t,1}[1 + \cos(\omega + \delta_1)] + V_{t,2}[1 - \cos(2\omega + \delta_2)] + V_{t,3}[1 + \cos(3\omega + \delta_3)]\} \tag{6}$$

$$U_{nb} = \sum_{i<j}\left[\frac{q_i q_j}{4\pi\varepsilon_0 r_{ij}} + 4\varepsilon_{ij}\left(\frac{\sigma_{ij}^{12}}{r_{ij}^{12}} - \frac{\sigma_{ij}^{6}}{r_{ij}^{6}}\right)\right] \tag{7}$$

where l denotes the distance between different bonding atoms; k_s denotes the force constant of the interatomic spring; k_b denotes the force constant between the bond angles; ω denotes the dihedral angle between four atoms; $V_{t,n}$ denotes the barrier height of the twisted potential energy; δ_n denotes the phase factor; n denotes the multiplicity of rotations related to the symmetry of the rotation of the dihedral angle; ε_0 denotes the potential trough.

https://doi.org/10.1021/acsomega.3c06390
ACS Omega 2024, 9, 11243−11254

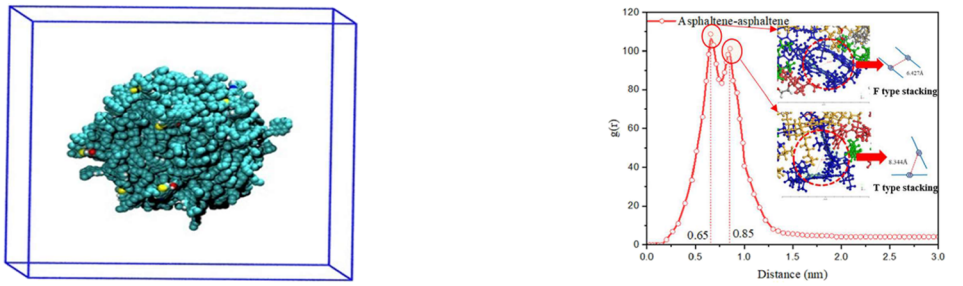

(a) Structure of ball models from oil sphere (b) RDF of asphaltene-asphaltene

Figure 6. Schematic diagram of the oil model.

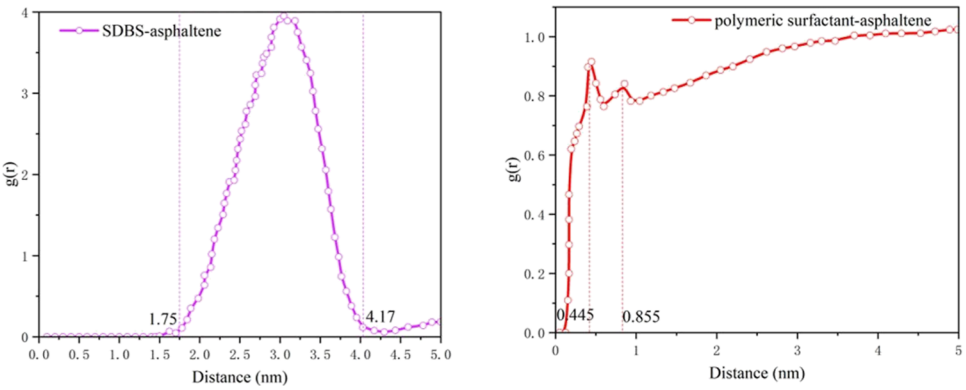

(a) RDF of SDBS-asphaltene (b) RDF of polymeric surfactant-asphaltene

Figure 7. RDF among particle pairs.

Eqs 4−7 represents the potential energy of bond stretching, bond angle bending, dihedral torsion, and nonbonding interactions, respectively. To better adapt to the OPLS-AA force field, TIP4P model can be adopted for water molecules.[45] In addition, to improve the calculation efficiency, the particle−particle-particle-mesh method can simulate the long-range static force.[46]

Molecular Calculation. The calculation of MD was carried out by the large-scale atomic/molecular massively parallel simulator (LAMMPS), as an opening source simulator and calculator.[47] The optimized oil−brine interfacial model was relaxed for 500 ps under NVT ensemble and a temperature of 328 K controlled by the Nose-Hoover algorithm. The initial oil−brine interfacial model was performed to discuss the effect of chemical agents through an MD simulation of 5 ns. The latest 1 ns was selected to analyze the occurrence state of chemical agents at the oil−brine interface. Finally, the results of MD simulation were presented and processed by Ovito Basic 3.7.5 as an opening source visual software.[48]

RESULTS AND DISCUSSION

Analysis from Molecular Perspective. After the relaxation process of the oil model, the asphaltene molecules impede the flow oil by aggregating in response to different stacking effects as shown in Figure 6. The adjacent asphaltene molecules interact through face-to-face stacking (F type stacking) and side-to-face stacking (T type stacking) at the distance of approximately 0.65 and 0.85 nm, respectively, which is dependent on the $\pi-\pi$ bond of the directional ring as shown in Figure 6b. Meanwhile, the electrostatic attraction among the resins also enhances the viscosity of the oil.

From the perspective of molecules, the stability of the molecular structure from the oil model is enhanced by the stacking effect from adjacent asphaltene molecules and the steric hindrance effect of other molecules. Thus, from a macroscopic perspective, it can be inferred that oil is more likely to exist in the pore. The asphaltene core needs to be separated to reduce its flow resistance. Therefore, measuring the distance among different distances can describe the viscosity reduction characteristics of oil. Through analyzing the RDF (radial distribution function), essential information on macromolecular structures around specific atoms can grasp the interaction between desired molecules as follows:[49]

After the relaxation of the oil−brine model with SDBS, the SDBS molecules are mainly distributed 3 nm away from the asphaltene molecules as shown in Figure 7a. The large distance between asphaltene and SDBS demonstrates that SDBS molecules are centrally adsorbed at the oil−water interface and cannot contact the asphaltene aggregated core. In contrast, there are obvious distributed peaks of molecules of the polymeric surfactant within the range 0.65 nm. Moreover, the molecules of the polymeric surfactant have similar numbers at different distances (0.85−5 nm) from asphaltene molecules. The distributing characteristics of the polymeric surfactant indicate that these molecules have entered the interior of the oil model and touches the asphaltene aggregated core, inducing the oil model to be more easily pulled by the polymeric surfactant and increasing its flow ability.

https://doi.org/10.1021/acsomega.3c06390
ACS Omega 2024, 9, 11243−11254

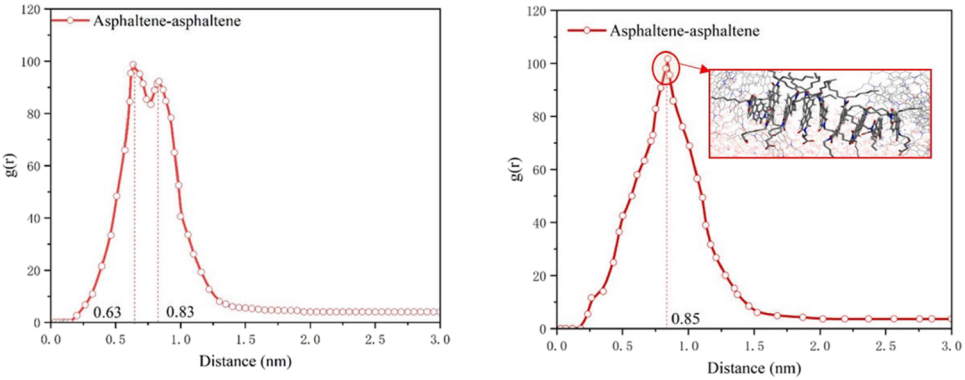

(a) Model with SDBS (b) Model with polymeric surfactant

Figure 8. RDF between asphaltene and asphaltene.

The distance between adjacent asphaltene molecules has been evidently enlarged, and only one peak remains at 0.85 nm under the influence of the polymeric surfactant, but this phenomenon has not repeatably occurred in the oil−brine model with SDBS molecules as shown in Figure 8. According to the analysis of the similar compatibility principle, the PB fragment of the polymeric surfactant molecules substituted polar groups into the oil model to promote the disintegration of the oil system and improve its migration, which provided a theoretical basis for the extraction of the remaining oil in blind-end pores.

Analysis of Production Performance. *Production Data of the Total Reservoir.* After various periods of displacement experiment, the production dynamic data of the heterogeneous reservoir are shown in Figure 9. After the injected volume

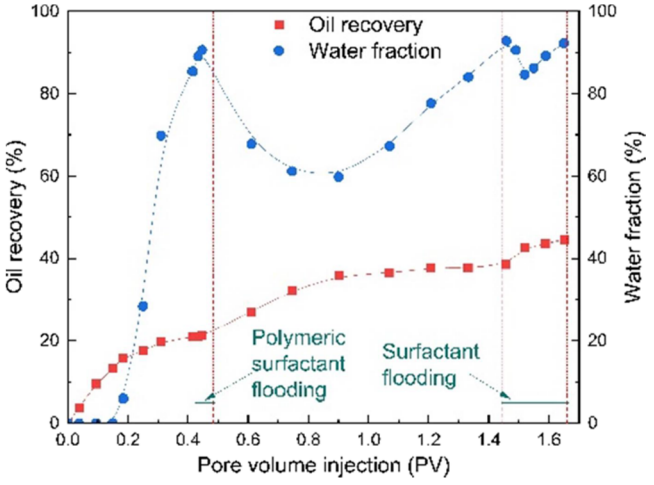

Figure 9. Production data of total period in the heterogeneous reservoir.

reached 0.18 PV, the water fraction of gradually exceeded 2% with the ending of water-less production period, and its increasing velocity of oil recovery was the greatest. At the conclusion of the water-less production period, the oil recovery only reached from 18 to 22% following hot brine flooding.

During the subsequent extraction period, oil recovery and water fraction did not vary evidently. And then, subsequent hot brine pushes the polymeric surfactant slug into the deep position, resulting in a long and dramatic reduction in the water fraction and promoting oil recovery to increase from 22 to 38%. Finally, the SDBS solution was injected into the simulated reservoir. The variation in water fraction during the ultimate extraction period was approximately 25% of that of the successive extraction period, but the alteration in oil recovery was roughly 40% of the previous period's value, demonstrating that the polymeric surfactant was able to prolong the extracting time.

Production Data in Different Layers. The alteration of water fraction, oil recovery, and percentage of liquid production with different layers are shown in Figure 10. During the primary extraction period (0−0.42 PV), the characteristics of water fraction in the MPL were similar to that of the HPL. In addition, the alteration characteristics of water fraction in the LPL during the subsequent and successive extraction periods were same as that of HPL (0.42−1.46 PV). Then, the polymeric surfactant slug entered the HPL and MPL, resulting in a decrease of water fraction. Meanwhile, the brine breakthrough of LPL occurred, leading to water fraction increasing rapidly.

The liquid production of different layers also reflects the adsorption ability and seepage resistance of different layers.[50] The liquid production was mainly contributed by the HPL at the beginning of the primary extraction period (0.05 PV). Then, the adsorption ability of the HPL gradually decreased because other layers diverted the injected fluid. After the polymeric surfactant slug was injected, the seepage resistance of the HPL and MPL gradually exceeded that of LPL, inducing a reversal of the liquid production ratio at the early stage of the subsequent extraction period.[51] After SDBS solution was injected, the above characteristics perform stable to maintain the highest value of the LPL in the percentage of liquid production.

The oil recovery of HPL and MPL increased rapidly before brine breakthrough. On the contrary, the LPL has a slow growth velocity during the primary extraction period. However, during the successive extraction periods, the oil recovery of the LPL (47.31%) surpassed those of the HPL (41.73%) and MPL (32.34%). After the SBDS solution was injected, only oil recovery of the LPL has an obvious increased performance compared to other layers. This phenomenon is related to the water channels with relatively low seepage resistance, inducing the injected fluid to easily enter into the LPL.[52]

Analysis of Macroscopic Distribution. *Primary Extraction Period.* Aside from the customary analysis of dynamic production data, the macroscopic fluid distribution alteration of the primary extraction period is shown in Figure 11. The important time nodes to observe the extracted performance in the primary extraction period are the brine existing near the injection well and the brine breakthrough in the production well.

https://doi.org/10.1021/acsomega.3c06390
ACS Omega 2024, 9, 11243−11254

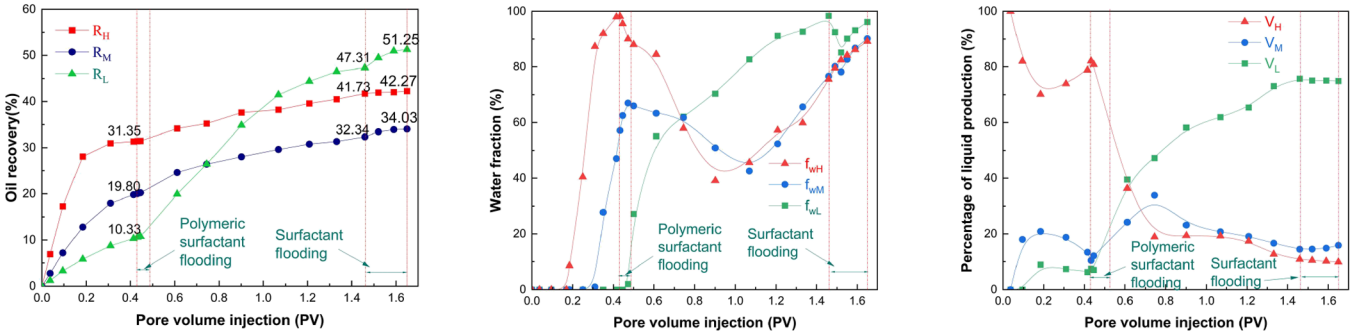

(a) Water fraction. (b) Percentage of liquid productio (c) Oil recovery.

Figure 10. Production performance in different layers.

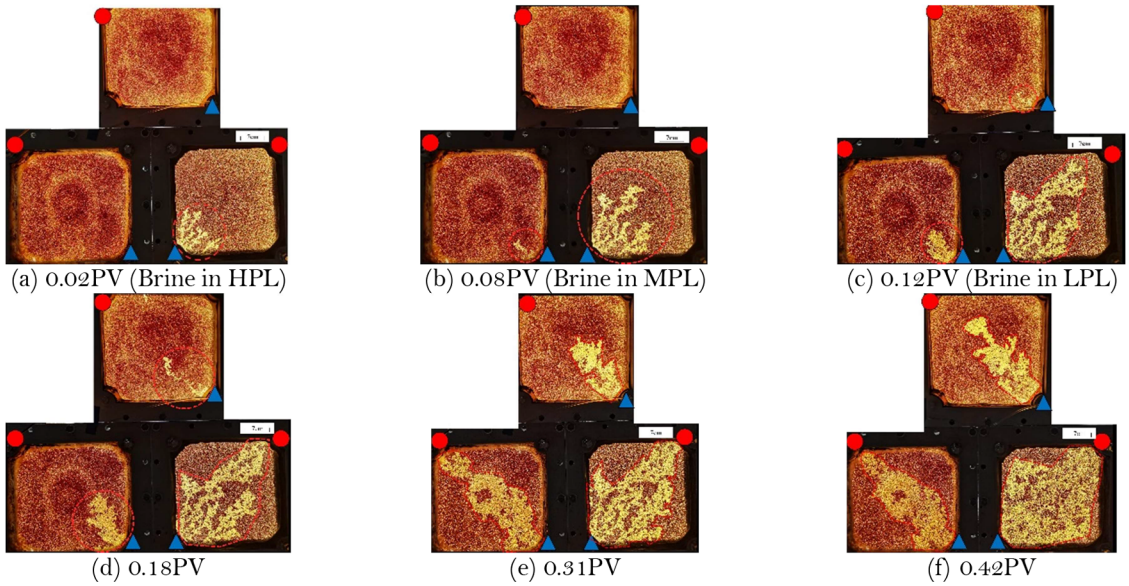

(a) 0.02PV (Brine in HPL) (b) 0.08PV (Brine in MPL) (c) 0.12PV (Brine in LPL)

(d) 0.18PV (e) 0.31PV (f) 0.42PV

Figure 11. Macroscopic distributed images during the primary extraction period.

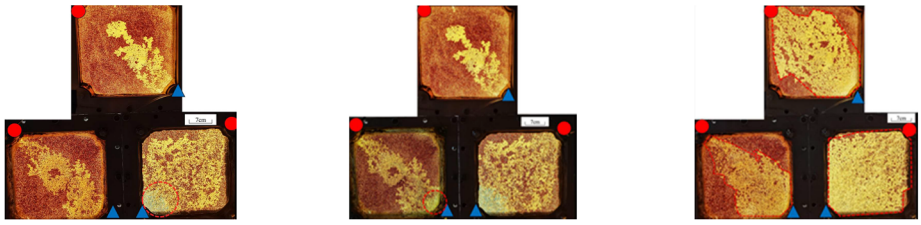

(a) Polymeric surfactant entered the HPL (0.43PV) (b) Polymeric surfactant entered the MPL (0.44PV) (c) The end state of successive extraction period (1.45PV)

Figure 12. Macroscopic distributed images during the subsequent and successive extraction periods.

As brine injection increased, flow channels were rapidly formed along the line between injection and production wells in the HPL and MPL as shown in Figure 11f. Following the establishment of flow channels, there was a rapid increase in the water fraction throughout the entire reservoir. Meanwhile, due to scouring by plenty of brine with low viscosity, much remaining oil with different types was left in the flow channels.

Due to the interlayer heterogeneity, the brine first entered into the layer with high permeability, which was called "tongued advance," while the flow channels formed rapidly along the line between the injection and production wells affected by viscosities of different fluids, which was called" viscous fingering."[53]

It is apparent that the penetration rate of the viscous fingering increases as the displacing front moves farther away from the injection well, indicating that the farther away from the injection wellhead, the longer the fingering distance per unit of time. Therefore, as shown in Figure 11f, the swept region around the production well was extremely narrow, while the swept region around the injection well was wide, showing obvious viscous fingering characteristics.

Subsequent and Successive Extraction Periods. The significant time nodes to observe the extracted performance in the subsequent and successive extraction periods are the polymeric surfactant existing near the injection well. To observe the distribution of the polymeric surfactant, the polymeric

https://doi.org/10.1021/acsomega.3c06390
ACS Omega 2024, 9, 11243−11254

surfactant solution was stained with a blue marker as shown in Figure 12. After the polymeric surfactant orderly entered into HPL and MPL, brine gradually entered into the LPL. The phenomenon of viscous fingering evidently occurred so that the flow channels quickly generated in the LPL to enlarge the swept region. The viscous fingering led to plenty of flake remaining oil in the LPL. It can also be demonstrated that the displacing fluid and the displaced fluid exhibit significant differences in mobility, which is evident from the observation that the polymeric surfactant did not participate deeply in fluid flow in the LPL.

Considering the viscosity of difference between the polymeric surfactant and brine in the heterogeneous reservoir, the velocity of the displacing front can be analyzed. The flow state of displacement front can be mechanically demonstrated by Figure 13. Because the width of the displacing front was smaller than

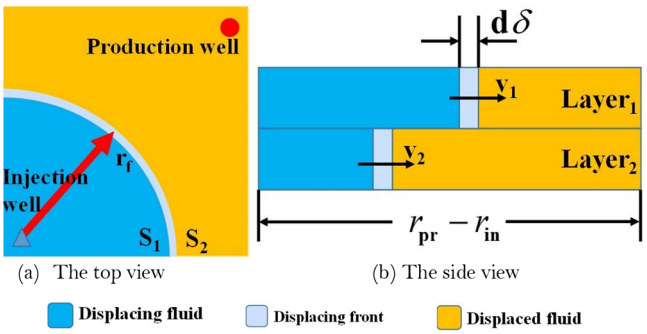

Figure 13. Schematic diagram of the flow mechanisms on the displacing front in different layers.

the displacing front radius, the region of displacing front can be simplified as

$$dS = S_1 - S_2 = \pi(r_f + \delta)^2 - \pi {r_f}^2 = 2\pi r_f\delta + \pi\delta^2 \approx 2\pi r_f\delta \tag{8}$$

Inspired by the equivalent seepage resistance method and Figure 13b, the mobility at the displacing front can be expressed as

$$\begin{cases} \dfrac{1}{\frac{r_D}{\lambda_1} + \frac{1-r_D}{\lambda_2}} = \dfrac{\lambda_1}{r_D + (1-r_D)M}, & r_D > 1 \\ \lambda_1, & r_D < 1 \end{cases} \tag{9}$$

If r_D exceeds 1, the displacing front arrives at the production well. According to Darcy's law and eq 11, the constitutive equation of displacing front can be mathematically expressed as

$$\frac{d\delta}{d\tau} = v_i = -\frac{k}{\mu}\frac{dP}{dr_f} = -\frac{k}{\phi(S_1 - S_2)}\lambda_f\frac{dP}{dr_f} \approx -\frac{k\lambda_f}{2\pi r_f\delta}\frac{dP}{dr_f} \tag{10}$$

Moreover, the formula for calculating the flow velocity without interlayer channeling before the displacing front reached the production well is as follows":

$$\frac{v_1}{v_2} = \frac{d\delta_1/d\tau}{d\delta_2/d\tau} = \frac{k_1\phi_2 r_{f2}}{k_2\phi_1 r_{f1}}\cdot\frac{r_{f2} + (1-r_{f2})M}{r_{f1} + (1-r_{f1})M} \tag{11}$$

When $k_1\phi_2/k_2\phi_1$ was set as 1, the flow velocity ratio between the displacing fluid and the displaced fluid can be expressed as

$$\frac{v_1}{v_2} = \frac{d\delta_1}{d\delta_2} = \frac{{r_{D2}}^2(1-M) + r_{D2}M}{{r_{D1}}^2(1-M) + r_{D1}M} \tag{12}$$

When the displacing front reached the production well in the first layer, the dimensionless displacing front radius of layer 1 is set as 1. Further, eq 12 can be simplified as

$$\frac{v_1}{v_2} = {r_{D2}}^2(1-M) + r_{D2}M \tag{13}$$

When the displacing front in the higher permeability layer reaches the production well, the displacing front of the lower permeability layer still has not reached and the flow velocity of the displacing front is highly sensitive to the location of the displacing front and the mobility ratio, as shown in Figure 14.

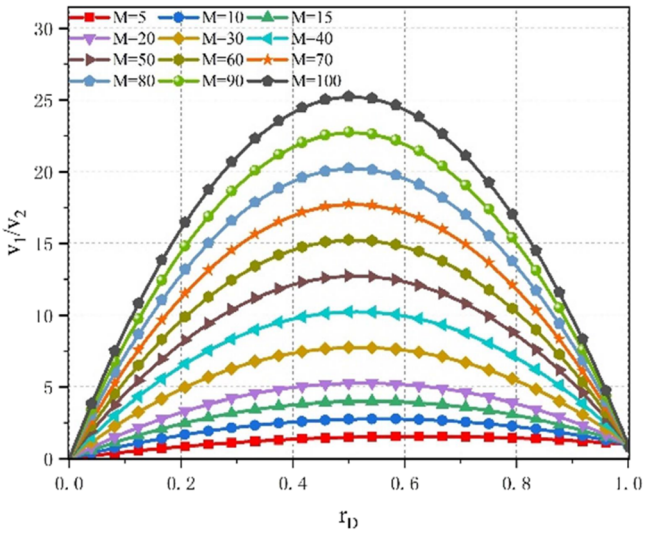

Figure 14. Relationship chart of the velocity ratio and the dimensionless displacing front radius.

When the mobility ratio has a small value, the difference in the flow velocity of different layers also becomes small, demonstrating that the displacing fronts in different layers reach the production well at similar times. Hence, the velocity ratio can be reduced by increased mobility ratio, inducing the polymeric surfactant easily into the HPL and MPL in a short time. Moreover, the increase of the mobility ratio can reduce the intensity of viscous fingering, which is conducive to expanding the swept region. Further, the influence of the swept region can be measured to describe the effect of the polymeric surfactant. The enlarged effect of the macroscopic swept region can be quantitatively described by sweep efficiency based on the identification of flow channels.

Compared with the sweep efficiency of HPL and MPL, the polymeric surfactant has an obvious effect on the spread of the swept region in the LPL as shown in Figure 11. Due to the increase of the sweep efficiency in the LPL, the sweep efficiency of the total reservoir approximately increased by 66.7%. In terms of the growth rate on production data as shown in Figure 10c, oil recovery (78%) was much greater than the sweep efficiency (10%) in the HPL during the successive extraction periods as shown in Figure 15. Similarly, the growth rate of oil recovery (139%) was also much greater than that of sweep efficiency (48%) in the MPL. However, the growth rate of oil recovery (300%) was less than that of sweep efficiency (484%) in the

https://doi.org/10.1021/acsomega.3c06390
ACS Omega 2024, 9, 11243−11254

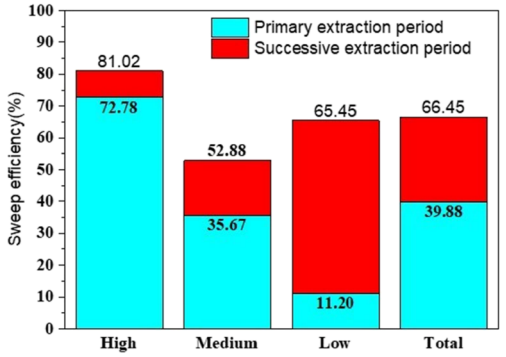

Figure 15. Alteration of sweep efficiency compared with primary and successive extraction periods.

LPL. To sum up, it can be found that the alteration amplitude between oil recovery and sweep efficiency is not coordinating.

Analysis of Microscopic Performance. After successive extraction periods, plenty of bluish spots with the polymeric surfactant existed in the swept region near the injection well of the HPL as shown in Figure 16a. When the polymeric surfactant aggregated in the swept regions to form bluish spots, some bluish clusters with spheroidal particles were left at the large pores, as shown in Figure 16b. Moreover, plenty of flaky remaining oil was extracted, and some corner oil was left in the closed pores, as shown in Figure 16c. During the subsequent and successive extraction periods, most of the membrane and columnar oil can be removed by emulsification and wettability alteration, enhancing the oil washing efficiency on the rock surface and large pores with favorable connectivity.

From the microscopic scale, the corner and blind-end remaining oil are left in the narrow, closed, and blind-end pores with poor connectivity to flow channels generated by brine flooding. The blind-end pores only have an opening side connecting with the flow channels so that the injected fluid cannot push the blind-end oil through the displacement pressure. Under the influence of the polymeric surfactant, the remaining oil in the blind-end pore was gradually extracted, and the interface of oil-aqueous gradually became depressed into the blind-end pore as shown in Figure 17.

Based on the results from MD simulation, the PB fragment of the polymeric surfactant gradually stretched and spread at the oil−water interface where the hydrophobic groups are embedded in the oil phase. Under low IFT of the oil−water interface by the polymeric surfactant, the increasing thickness of the oil membrane gradually induces the rise of the gradient of the local IFT, thereby generating Marangoni effect from the region around the blind-end.[54,55] Thus, the blind-end oil was gradually activated to extract the remaining oil far from the rock surface. While the remaining oil near the rock surface was not extracted in time, the depressing interface of oil−water inverted into the membrane oil. The concave interface by the Marangoni effect was clearly different from the protruding interface by the pulling effect of polymeric chains in the blind-end model as shown in Figure 18.

These oil extraction effects in the blind-end pore employed different types of energy sources and have an important influence on the interface morphology. From the recognition of MD simulation for molecules of polymeric surfactant embedded in the oil model, the oil migration with polymeric surfactant as brine moves is called the pulling effect. The pushing effect is derived from the stored elastic energy generated by the cohesive energy of the polymeric surfactant. And its extracted effectiveness is contingent upon the compatibility between the surfactant and the remaining oil. In contrast, Marangoni effect can promote the transformation of interfacial energy to displacement kinetic energy by the emulsification of the oil−water interface.[56,57] The blind-end remaining oil was dragged into the flow channels by the Marangoni flow with the polymeric surfactant to form the O/W emulsion or movable remaining oil.[58,59]

During the subsequent and successive extraction periods, the pulling effect and Marangoni effect of the polymeric surfactant synergistically promote the oil extraction of blind-end pores. Comparison of the effect of polymeric surfactant and SDBS in the blind-end pore, the reduction of IFT of oil−water forms an interfacial gradient and generates a new displacement energy source, leading to enhancements in the effectiveness of oil recovery. Under the pulling effect of the polymeric surfactant, the immobile remaining oil can be extracted from blind-end or other multitype pores.

CONCLUSIONS

In this work, we discussed the EOR mechanism of the polymeric surfactant in heterogeneous reservoirs based on MD simulation and visualization experiment. The following conclusions are made:

- The MD simulation of the oil−brine interface model demonstrates that some fragments of polymeric surfactant molecules substitute polar groups into the oil model to promote the disintegration of the oil system and improve its migration.
- The intensity of tongued advance is significantly determined by the velocity of the displacement front, which can be directly by the velocity ratio from the mathematical model and the injected volume from the extracted experiment.
- When the displacing front in the layer with great permeability arrives at the production well, the velocity ratio generated by tongued advance also depends on the position of the displacing front and the mobility ratio. Particularly, when the displacing front is situated in the

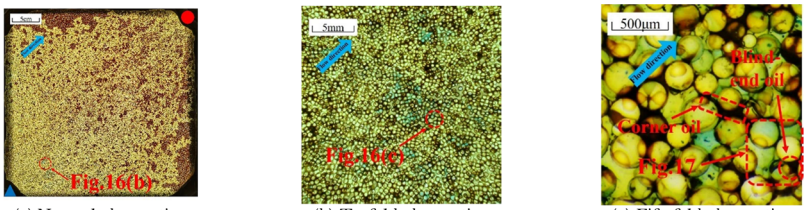

(a) Normal observation (b) Tenfold observation (c) Fiftyfold observation

Figure 16. Distribution diagram of the polymeric surfactant in HPL at different scales.

https://doi.org/10.1021/acsomega.3c06390
ACS Omega 2024, 9, 11243−11254

(a) Initial state (b) Middle state (c) Ultimate state

Figure 17. Dynamic extracted alteration of blind-end oil on the microscale.

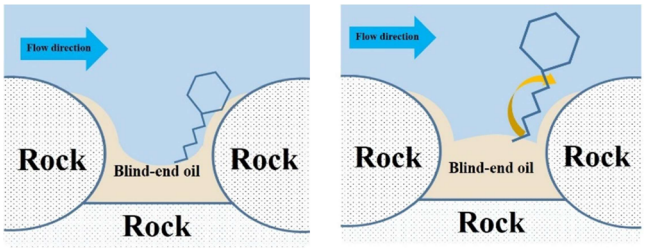

(a) Marangoni effect (b) Pulling effect

Figure 18. Schematic diagram of blind-end oil extraction by the polymeric surfactant.

middle of the formation, the velocity ratio among different layers is the greatest.

- Reducing the mobility ratio can achieve a significant goal on weakening the strength of viscous fingering occurring along the injection-production well lines and tongued advance occurring among the different layers, which can be advantageous in enlarging the swept region.
- Polymeric surfactant can reduce the IFT at the oil−water interface and can emulsify oil to reduce its seepage resistance. Meanwhile, the IFT reduction promotes the transformation of interfacial energy to displacement kinetic energy so that some remaining oil can be easily extracted from blind-end pores.

AUTHOR INFORMATION

Corresponding Author

Huiqing Liu − *State Key Laboratory of Petroleum Resources and Prospecting, China University of Petroleum, Beijing 102249, China*; Email: 1140369688@qq.com

Authors

Hao Zheng − *State Key Laboratory of Petroleum Resources and Prospecting, China University of Petroleum, Beijing 102249, China; CNOOC International Limited, Beijing 100026, China*

Kaijun Tong − *CNOOC International Limited, Beijing 100026, China*

Complete contact information is available at: https://pubs.acs.org/10.1021/acsomega.3c06390

Author Contributions

H.Z.: Methodology, investigation, and writing - original draft. H.L.: Supervision- review and editing. K.T.: Conceptualization, investigation, and software.

Notes

The authors declare no competing financial interest.

ACKNOWLEDGMENTS

The authors are grateful to Mr. Yu Li for the support of visual displacement images. This work is also supported by the National Natural Science Foundation of China Joint Fund Project (no.U20B6003) and the China Petroleum Chemical Corporation (P22174).

NOMENCLATURE

k	Permeability
P_{in}	Pressure of injection well
r_D	Dimensionless displacing front radius
S	Sweep area of displacing front
δ	Penetration distance
μ	Viscosity of fluid
ϕ	Porosity
M	Mobility ratio
P_{pr}	Pressure of production well
r_f	Location of displacing front
v_i	Velocity of displacing front
λ	Mobility
τ	Time of fluid migration
ω	Dihedral angle between four atoms

REFERENCES

(1) Tavakoli, V. *Carbonate reservoir heterogeneity: overcoming the challenges*; Springer Nature, 2019.

(2) Chen, X.; Li, Y. Q.; Liu, Z. Y. Experimental investigation on the enhanced oil recovery efficiency of polymeric surfactant: Matching relationship with core and emulsification ability. *Pet. Sci.* **2022**, *20*, 619 DOI: 10.1016/j.petsci.2022.11.002.

(3) Ma, Z.; Leung, J. Y. Design of warm solvent injection processes for heterogeneous heavy oil reservoirs: A hybrid workflow of multi-objective optimization and proxy models. *J. Pet. Sci. Eng.* **2020**, *191*, No. 107186.

(4) He, J.; Liu, X.; Zhu, X. Water-flooding characteristics of lithologic reservoir in Ordos basin. *Sci. Rep.* **2021**, *11*, 2503.

(5) Xu, F.; Song, X.; Song, Z. Heat extraction and interlayer interference in heterogeneous multi-layer commingled production oil reservoir. In *56th US Rock Mechan- ics/Geomechanics Symposium*, 2022.

(6) Wang, Q.; Yang, S.; Lorinczi, P. Experimental investigation of oil recovery performance and permeability damage in multilayer reservoirs after CO2 and water−alternating-CO2 (CO2−WAG) flooding at miscible pressures. *Energy Fuels* **2019**, *34*, 624−636.

(7) He, L.; Xiaohan, P.; Kai, L. Current status and trend of separated layer water flooding in China. *Pet. Explor. Dev.* **2013**, *40*, 785−790.

(8) Wang, F. S.; Xu, D. K.; Yu, L. *The Full-Automatic Real-Time Display, Testing and Adjustable System in Separated Layers Water Injection Well*; SPE Intelligent Energy International, 2012.

(9) Zhang, L.; Xu, C.; Zhang, K. Production optimization for alternated separate-layer water injection in complex fault reservoirs. *J. Pet. Sci. Eng.* **2020**, *193*, No. 107409.

(10) Rezaeiakmal, F.; Parsaei, R.; Shafiabadi, A. Insights into the flow behaviour of the pre- generated polymer enhanced foam in heterogeneous porous media during tertiary oil recovery: Effect of gravitational forces. *J. Pet. Sci. Eng.* **2022**, *213*, No. 110385.
(11) Wang, W.; Peng, Y.; Chen, Z. Synergistic Effects of Weak Alkaline−Surfactant−Polymer and SiO2 Nanoparticles Flooding on Enhanced Heavy Oil Recovery. *Energy Fuels* **2022**, *36*, 7402−7413.
(12) Aitkulov, A.; Mohanty, K. K. Investigation of alkaline-surfactant-polymer flooding in a quarter five-spot sandpack for viscous oil recovery. *J. Pet. Sci. Eng.* **2019**, *175*, 706−718.
(13) Ding, M.; Wang, Y.; Li, Z. The role of IFT and emulsification in recovering heavy oil during S/SP flooding. *J. Ind. Eng. Chem.* **2019**, *77*, 198−208.
(14) Gao, Q.; Zhong, C.; Han, P. Synergistic effect of alkali−surfactant−polymer and pre-formed particle gel on profile control after polymer flooding in heterogeneous reservoirs. *Energy Fuels* **2020**, *34*, 15957−15968.
(15) Dong, X.; Liu, H.; Chen, Z. Enhanced oil recovery techniques for heavy oil and oilsands reservoirs after steam injection. *Appl. Energy* **2019**, *239*, 1190−1211.
(16) Khamees, T.; Flori, R. Investigating the propagation of the colloidal dispersion gel (CDG) in thick heterogeneous reservoirs using numerical simulation. *Am. J. Sci. Eng. Technol.* **2019**, *4*, 1−17.
(17) Lashari, N.; Ganat, T. Emerging applications of nanomaterials in chemical enhanced oil recovery: Progress and perspective. *Chinese Journal of Chemical Engineering* **2020**, *28*, 1995−2009.
(18) Li, J.; Jiang, H.; Hou, J. The effects of oil displacement efficiency and conformance efficiency on viscosity of asp flooding in a heterogeneous reservoir. *Pet. Sci. Technol.* **2014**, *32*, 830−839.
(19) Haydon, D. A. An investigation of droplet oscillation during mass transfer I. The conditions necessary, and the source of the energy for the oscillations. *Proc. R. Soc. Lond. Ser A. Math. Phys. Sci.* **1958**, *243*, 483−491.
(20) Davies, T.; Haydon, D. A. An investigation of droplet oscillation during mass transfer II. A dynamical investigation of oscillating spherical droplets. *Proc. R. Soc. Lond. Ser. A. Math. Phys. Sci.* **1958**, *243*, 492−499.
(21) Ross, S.; Haak, R. Inhibition of foaming. IX. Changes in the rate of attaining surface tension equilibrium in solutions of surface-active agents on addition of foam inhibitors and foam stabilizers. *J. Phys. Chem.* **1958**, *62*, 1260−1264.
(22) Masoudi, M.; Khosravi, M.; Rostami, B. Effect of B′enard-Marangoni flow on the by-passed oil recovery: Micromodel study. *J. Pet. Sci. Eng.* **2019**, *178*, 1067−1078.
(23) Huang, Z.; Li, D.; Jian, Q.; et al. Thermal and hydraulic analysis of ultra-thin vapor chamber with copper columns considering Marangoni effect. *Int. J. Heat Mass Transfer* **2022**, *184*, No. 122343.
(24) Wang, D.; Cheng, J.; Xia, H. Viscous-elastic fluids can mobilize oil remaining after water-flood by force parallel to the oil-water interface. In *SPE Asia Pacific Improved Oil Recovery Conference*, 2001.
(25) Hashemi, L.; Blunt, M.; Hajibeygi, H. Pore-scale modelling and sensitivity analyses of hydrogen-brine multiphase flow in geological porous media. *Sci. Rep.* **2021**, *11*, 8348.
(26) Li, Y.; Liu, H.; Wang, W.; Loh, W. L.; Lyu, X.; Li, X.; Peng, C.; Peng, H. Microvi- sual Investigation on Steam-Assisted Heavy Oil Extraction Behavior in Heterogeneous Porous Media. *Energy Fuels* **2023**, *37*, 11776−11786.
(27) Jia, H.; Lian, P.; Yan, H.; Yuan, J.; Tang, H.; Wei, X.; Song, J.; He, J.; Lv, K.; Liu, D. Novel molecular insight into the discrepant distributions for ionic surfactants in light oil/water and heavy oil/water systems. *Fuel* **2021**, *304*, No. 121460.
(28) Lu, N.; Dong, X.; Liu, H.; Chen, Z.; Xu, W.; Zeng, D. Molecular insights into the synergistic mechanisms of hybrid CO2-surfactant thermal systems at heavy oil-water interfaces. *Energy* **2024**, *286*, No. 129476.
(29) Sun, H.; Li, X.; Liu, D.; Li, X. Synergetic adsorption of asphaltenes and oil displace- ment surfactants on the oil-water interface: Insights on stabilization mechanism of the interfacial film. *Chem. Eng. Sci.* **2021**, *245*, No. 116850.
(30) Wu, D.; Liu, Y.; Lu, X. Study on Blockage and Fluid Diversion Behaviors of Polymer Microspheres. In *SPE EuropEC-Europe Energy Conference featured at the 83rd EAGE Annual Conference & Exhibition*, 2022.
(31) Wang, Y.; Liu, H.; Chen, Z. A visualized investigation on the mechanisms of anti-water coning process using nitrogen injection in horizontal wells. *J. Pet. Sci. Eng.* **2018**, *166*, 636−649.
(32) Xiaohu, D.; Jian, W.; Huiqing, L. SAGD scaled physical simulation experiment for oilsands reservoirs with high water-bearing layer. *Acta Pet. Sin.* **2022**, *43*, 658.
(33) Habib, R.; Karimi, N.; Yadollahi, B. A pore-scale assessment of the dynamic response of forced convection in porous media to inlet flow modulations. *Int. J. Heat Mass Transfer* **2020**, *153*, No. 119657.
(34) Gholinezhad, S.; Kantzas, A.; Bryant, S. L. Effect of surface functionalized silica nanoparticles on interfacial behavior: Wettability, interfacial tension and emulsifica- tion characteristics. *J. Mol. Liq.* **2022**, *349*, No. 118220.
(35) Pratama, R. A.; Babadagli, T. Reconsideration of steam Additives to improve displace- ment efficiency: can new generation chemicals be solution for steam induced unfavorable wettability alteration? In *SPE Annual Technical Conference and Exhibition*, 2019.
(36) Wu, Z.; Wang, L.; Xie, C. Experimental investigation on improved heavy oil recovery by air assisted steam injection with 2D visualized models. *Fuel* **2019**, *252*, 109−115.
(37) Pratama, R. A.; Babadagli, T. Wettability state and phase distributions during steam injection with and without chemical additives: An experimental analysis using visual micromodels. *SPE Reservoir Evaluation & Engineering* **2020**, *23*, 1133−1149.
(38) Wang, Y.; Liu, H.; Wang, J. Formulation development and visualized investigation of temperature-resistant and salt-tolerant surfactant-polymer flooding to enhance oil recovery. *J. Pet. Sci. Eng.* **2019**, *174*, 584−598.
(39) Feng, L.; Manica, R.; Lu, Y. Effect of sodium citrate on asphaltene film at the oil−water interface. *J. Colloid Interface Sci.* **2022**, *625*, 24−32.
(40) Lu, N.; Dong, X.; Chen, Z. Effect of solvent on the adsorption behavior of asphaltene on silica surface: A molecular dynamic simulation study. *J. Pet. Sci. Eng.* **2022**, *212*, No. 110212.
(41) Tang, J.; Qu, Z.; Luo, J. Molecular dynamics simulations of the oil-detachment from the hydroxylated silica surface: effects of surfactants, electrostatic interactions, and water flows on the water molecular channel formation. *J. Phys. Chem. B* **2018**, *122*, 1905−1918.
(42) Wang, S.; Wang, J.; Liu, H. Q. Impacts of inorganic salts ions on the polar components desorption efficiency from tight sandstone: A molecular dynamics simulation and QCM- D study. *Pet. Sci.* **2022**, *19*, 900−915.
(43) Ge, Y.; Zhu, Q.; Li, Y. An electrostatic-variable coarse-grained model for predicting en- thalpy of vaporization, surface tension, diffusivity, conductivity, and dielectric constant of aqueous ionic liquid. *J. Mol. Liq.* **2022**, *346*, No. 118230.
(44) Fan, X.; Shang, H.; Li, J. Effects of microwave electric field on the structure and association behaviour of asphaltenes: MD and DFT study. *Chem. Eng. Sci.* **2023**, *265*, No. 118245.
(45) Benavides, A.; Portillo, M.; Chamorro, V. A potential model for sodium chloride solutions based on the TIP4P/2005 water model. *J. Chem. Phys.* **2017**, *147*, 104501.
(46) Aminian, A.; ZareNezhad, B. Oil-detachment from the calcium carbonate surfaces via the actions of surfactant, nanoparticle and low salinity brine: an insight from molecular dynamic simulation. *Chem. Eng. Sci.* **2019**, *202*, 373−382.
(47) Plimpton, S. Fast parallel algorithms for short-range molecular dynamics. *J. Comput. Phys.* **1995**, *117*, 1−19.
(48) Xu, N.; Liu, Z.; Liu, F. Impacts of iron rust particle and weak alkalinity on surfactant micelle structure and drag reduction ability. *Phys. Chem. Chem. Phys.* **2023**, *25*, 6002−6008.
(49) Ahmadi, M.; Chen, Z. Comprehensive molecular scale modeling of anionic surfactant- asphaltene interactions. *Fuel* **2021**, *288*, No. 119729.

https://doi.org/10.1021/acsomega.3c06390
ACS Omega 2024, 9, 11243−11254

(50) Imqam, A.; Bai, B. Optimizing the strength and size of preformed particle gels for better conformance control treatment. *Fuel* **2015**, *148*, 178−185.
(51) Selem, A. M.; Agenet, N.; Gao, Y. Pore-scale imaging and analysis of low salinity waterflooding in a heterogeneous carbonate rock at reservoir conditions. *Sci. Rep.* **2021**, *11*, 15063.
(52) Pei, H.; Zhang, G.; Ge, J. Comparative effectiveness of alkaline flooding and alkaline− surfactant flooding for improved heavy-oil recovery. *Energy Fuels* **2012**, *26*, 2911−2919.
(53) Al-Shalabi, E. W.; Ghosh, B. Effect of pore-scale heterogeneity and capillary-viscous fingering on commingled waterflood oil recovery in stratified porous media. *J. Pet. Eng.* **2016**, *2016*, No. 1708929, DOI: 10.1155/2016/1708929.
(54) Chen, I.-C.; Akbulut, M. Nanoscale dynamics of heavy oil recovery using surfactant floods. *Energy Fuels* **2012**, *26*, 7176−7182.
(55) Yu, F.; Jiang, H.; Fan, Z. Formation and flow behaviors of in situ emulsions in heavy oil reservoirs. *Energy Fuels* **2019**, *33*, 5961−5970.
(56) Nakache, E.; Dupeyrat, M.; Vignes-Adler, M. The contribution of chemistry to new Marangoni mass-transfer instabilities at the oil/water interface. *Faraday Discuss. Chem. Soc.* **1984**, *77*, 189−196.
(57) Pratt, H. Marangoni flooding with water drives: A novel method for EOR? In *SPE Asia- Pacific Conference*, 1991.
(58) Wang, D.; Cheng, J.; Yang, Q. Viscous-elastic polymer can increase microscale dis- placement efficiency in cores. In *SPE annual technical conference and exhibition*, 2000.
(59) Zhang, D.; Du, X.; Song, X.; Wang, H.; Li, X.; Jiang, Y.; Wang, M. Application of the marangoni effect in nanoemulsion on improving waterflooding technology for heavy-oil reservoirs. *SPE Journal* **2018**, *23*, 831−840.

https://doi.org/10.1021/acsomega.3c06390
ACS Omega 2024, 9, 11243−11254